Flexible Spatial Light Modulator Based Coupling Platform for Photonic Integrated Processors

Cátia Pinho[1,2], George S. D. Gordon[4], Berta Neto[1], Tiago M. Morgado[1], Francisco Rodrigues[1,3], Ana Tavares[1,3], Mário Lima[1,2], Timothy D. Wilkinson[4], António Teixeira[1,2]

[1] Instituto de Telecomunicações (IT), University of Aveiro, Aveiro, 3810-193, Portugal
[2] Department of Electronics, Telecommunications and Informatics (DETI), University of Aveiro, Portugal
[3] PICadvanced, University of Aveiro, Incubator, PCI – Creative Science Park Via do Conhecimento, Ílhavo, Portugal
[4] Electrical Division, Engineering Department, University of Cambridge, 9, JJ Thomson Avenue, Cambridge, UK
e-mail: catiap@ua.pt, gsdg2@cam.ac.uk, bneto@av.it.pt, tmcm@ua.pt, francisco@picadvanced.com, ana@picadvanced.com, mlima@ua.pt, tdw13@cam.ac.uk, teixeira@ua.pt

Abstract — **Enhanced Photonic Integrated Circuits (PIC) are required for the current demand of flexibility and reconfigurability in telecommunications networks. However, the technical and functional requirements of the PIC demand a thorough characterization and testing to provide an accurate prediction of the PIC performance. In the characterization and testing context, the use of Spatial Light Modulator (SLM) can be beneficial. SLM is a diffractive device to reconstruct images from Computer Generated Holograms (CGH) that allows to modulate the wavefront of a light beam. This capability can be explored to feed/receive optical signals to the PIC, i.e., as a flexible SLM based coupling platform. The feasibility of this approach was tested with the generation of a multiplexing/demultiplexing CGH to be applied into an optical chip for data compression based on Haar wavelet transform. Simulation results for building blocks as well as the all-optical network for the optical data compression chip are presented, supporting their theoretical feasibility. A new concept to use a SLM as a flexible coupling platform to complement PIC characterization process is proposed and a Haar transform data compression PIC described.**

Keywords - photonic integrated circuits (PIC); integrated optics; spatial light modulator (SLM); computer generated holography (CGH); all-optical devices; Haar transform.

I. INTRODUCTION

In the recent years, we have witnessed a significant increase in the data traffic, which the traditional copper based electronic media fail to carry [1]–[3]. Furthermore, the increasing demand for higher image/video storage capacity and data transmission rates led to the search of new bandwidth optimization solutions. Integrated photonics appears as a promising technology to achieve this outcome. Photonic Integrated Circuits (PIC) are the equivalent of Electronic Integrated Circuits (EIC) in the optical domain. As an alternative to transistors and other electronic components, PIC contain optical elements, such as modulators, detectors, attenuators, multiplexers, optical amplifiers and lasers. PIC advantages can be attributed to their lower power consumption, smaller volume and weight, higher thermal and mechanical stability, and the easier assembly of numerous and complex systems. In summary, PIC-based optical communication systems offer an efficient and cost-effective solution to data transmission driving to a significant boost in the segment [2]. An annual growth rate of 25.2% in the PIC market during the period of 2015 to 2022 is foreseen [3]. There is also an increasing demand for PIC driven by innovative applications in biophotonics [2].

PIC can be characterized as a multiport device composed of an integrated system of optical elements embedded onto a single chip using a waveguide architecture [4]. The testing of optical components is more difficult than on electrical components and for an accurate prediction of the PIC performance, an extensive characterization/testing is required [5]. Moreover, optical component testing is difficult and time-consuming, e.g., due to the tight 3D alignment tolerances for accurate coupling of light [5].

Given increasing demand for data transmission and storage, data compression emerges as an important field of study with different available techniques explored to release additional bandwidth. Specifically, for faster image processing, compression methods are fundamental tools to decrease redundant data. Different compression transformation techniques can be used, with the wavelet-based transforms as the most promising ones due to their simplicity and fast computation [6]. All-optical network design appears as a prominent solution for the application of such compression methods. By applying this architecture into a PIC, image compression can be attained with lower cost, less power consumption and high data rate due to an all-optical processing implementation [7]. Among the wavelet-based methods, Haar transform (HT) offers a good approach for image processing and pattern recognition due to its simple design, fast computation power and efficiency, being easily implemented by optical planar interferometry [4] [6] [7]. The HT implementation can be achieved with a two level network of asymmetric coupler devices [4].

The capability of a Spatial Light Modulator (SLM) to dynamically reconfigure the optical wavefronts makes it an attractive technology to excite cores or modes of optical waveguides [8] [9], as it allows the arbitrary addition or

removal of channels by the software and it is anticipated that it can achieve some basic channel equalization. This feature can then be explored to feed/receive optical signal from PIC [1].

SLM is an electronically programmable device that modulates light using an array of reconfigurable pixels [10]. This device can control incident light in amplitude-only, phase-only or a combination of phase-amplitude [10] [11]. One of the most commonly used modulation mechanisms is the electro-optical SLM containing liquid crystals as the modulation material [11] [12]. The liquid crystal spatial light modulators have a microdisplay that is used to collect and modulate the incident light, in a transmissive (liquid crystal display – LCD) or reflective (Liquid Crystal on Silicon – LCoS) form. Another distinguishing characteristic of these modulators is the alignment of the liquid crystal molecules, which is typically either parallel, vertical, or with twisted formation. In combination with appropriate polarizing optics, this determines which properties of the incident light beam can be altered, i.e., phase, amplitude or a combination of the two [11] [12].

Nonetheless, common hologram generation methods cannot arbitrarily modulate the amplitude and phase of a beam simultaneously [13] [14]. It is not then possible to simply address the inverse Fourier transform of the desired pattern into the far-field and replicate the resulting distribution of amplitude and phase directly on the SLM [13]. Thus, it is necessary to apply optimization algorithms to calculate the best hologram possible within the constraints of the device [13].

The SLM based on nematic LCoS technology is an electrically addressed reflection type phase-only SLM in which the liquid crystal is controlled by a direct and accurate voltage and can modulate the wave front of a light beam [11] [15], as shown in Figure 1.

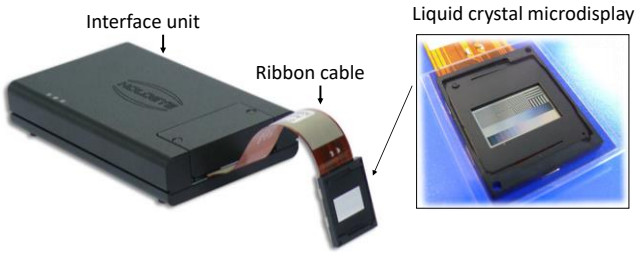

Figure 1. LCOS SLM Pluto phase modulator from Holoeye © 2018 Holoeye Photonics AG.

LCoS SLM is used as a diffractive device to reconstruct images from Computer Generated Holography (CGH) [16]. Appropriate holograms can be generated using a range of different optimization techniques, e.g., linear Fourier transform (i.e., linear phase mask) [17][18], Iterative Fourier Transform Algorithm (IFTA) [19] [20], Gerchberg-Saxton algorithm [21] and simulated annealing [22]. The use of a SLM as a diffractive device to reconstruct images from CGH allows to modulate the wavefront of a light beam.

In this study, we proposed the use of the SLM technology as a flexible coupling platform for feeding photonic integrated processors, i.e., to feed/receive optical signal from a PIC [1]. Furthermore, it can be used as a parallel implementation of the HT image compression algorithm. Preliminary results were obtained to produce an expected CGH to be applied into an optical chip for data compression based on Haar wavelet transform [1].

The paper is organized in four sections. Section II describes the methodology applied for the design of the HT two level network, building blocks, and PIC; the generation of the CGH; and the setup for the flexible SLM coupling platform. Subsection II-A presents the all-optical system architecture for data compression based in HT; Subsection II-B presents the design of the PIC for data compression, addressing the asymmetric coupler and chip design; Subsection II-C presents the generation and optimization of the CGH. Sections III and IV present the obtained results and its discussion, respectively. Section V concludes the study.

II. METHODOLOGY

The methodology is divided into three subsections: (A) the design of an all-optical system architecture for data compression based in Haar wavelet transform; (B) the algorithms used for the generation and optimization of the CGH; and (C) the implementation of the SLM setup to acquire the CGH.

A. *All-optical system architecture for data compression based in HT*

A digital image can be seen as a group of pixels, where neighboring pixels are correlated and usually redundant. Through the decreasing of this redundancy (by compression techniques) the transmission speed and the bandwidth of the system can be optimized. Transforms based on orthogonal functions are the most frequently used in signal compression techniques. The orthogonality is an important property for multi-resolution analysis, where the original signal can be split into low and high frequency components without duplicating information. These functions only require subtractions and additions for their forward and inverse transforms. Examples of these transforms are the Discrete Fourier Transform (DFT), the Discrete Cosine Transform (DCT), and the Discrete Wavelet Transforms (DWT) [23]. DWT have the advantage of representing a fundamental tool for local spectral decomposition and nonstationary signal analysis, used in the JPEG2000 standard as wavelet-based compression algorithms [24]. DWT represent an image as a sum of wavelet functions, with different location and scale [25], i.e., High-pass (detail) and Low-pass (approximate) coefficients. Low-Pass (LP) and High-Pass (HP) filters are applied to the input data with a two level signal decomposition architecture, as depicted in Figure 2.

The Haar wavelet transforms [7] [26] [27] (an example of multiresolution analysis) were chosen due to their simplicity and fast computation.

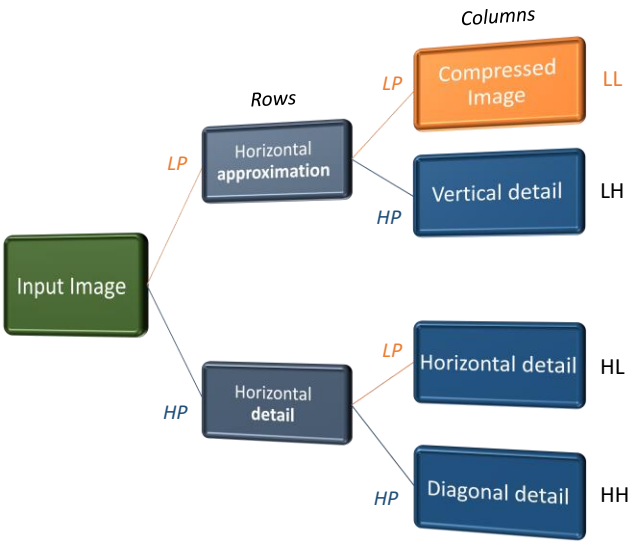

Figure 2. Two level band decomposition using multi-resolution analysis based on wavelet transform. Low-Pass (LP) and High-Pass (HP) filters are applied two times to obtain the 1D transform (L and H components) and the 2D transform (LL, LH, HL and HH components).

The sub-band decomposition achieved through the wavelet transform enables the compression directly on a specific portion of the spectrum, through spatial frequency characterization.

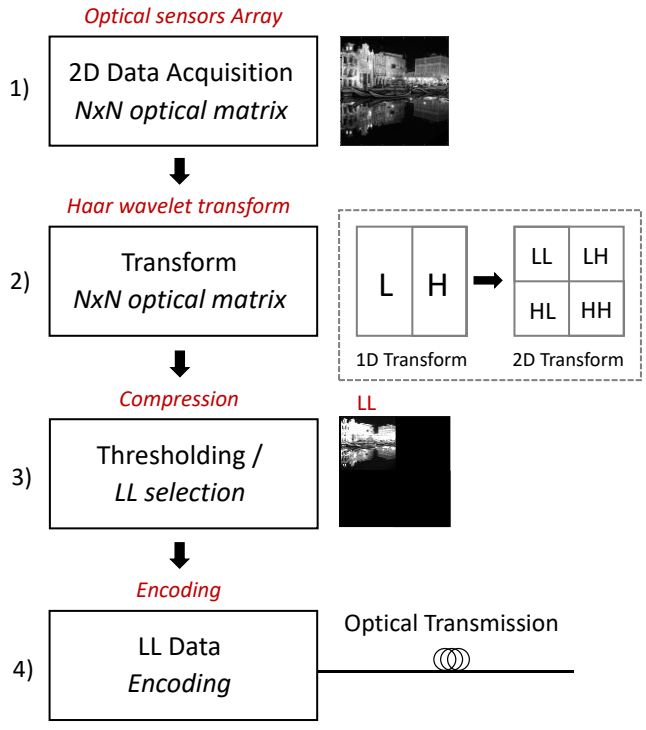

Figure 3. All-optical scheme of system building blocks for Haar wavelet transform processing and compression. 2D transform process schematic describes Low-pass (L) and High-pass (H) filtering through sub-band decomposition [7].

The all-optical system architecture for data compression based in the HT can be divided in four main building blocks: i) optical sensors array; ii) Haar wavelet transform; iii) compression; and iv) data encoding section.

The scheme for all-optical image acquisition, processing, and transmission is depicted in Figure 3.

The first building block entails the acquisition level with optical sensors for light detection and two dimensional (2D) data sampling. The HT is implemented in the second building block, to extract the image properties by exploiting the energy compaction features of the wavelet decomposition.

The HT block (second building block) includes Low-pass (L) and High-pass (H) filters associated with the Haar wavelet, applied over one dimension (1D) at time. The filtering operation can be simplified as the calculation of the average between two neighbors' pixels values (LP) or the difference between them (HP). Equation (1) presents the Haar transform scattering matrix for a generic 1D input (a_i coefficients), i.e., pixel line or column. LP and HP filters are applied two times to obtain the 1D transform (L and H component) and the 2D transform with the four LL, LH, HL and HH components, see Figure 2 and Figure 3.

The coefficients on the left side of (1) are the scaling c_{ij} and detail d_{ij} coefficients (where i refers to the transform level and j to the coefficient index) obtained from the LP and HP filtering, respectively, for each pixel pair, which corresponds to the 1D first level of the Haar discrete wavelet transform. In a 2D matrix input ($N \times N$) this operation is performed twice, i.e., horizontally and vertically, for each transformation level, to guarantee that image intensity variations are evaluated along the two dimensions.

$$\begin{bmatrix} \vdots \\ c_{10} \\ d_{10} \\ c_{11} \\ d_{11} \\ c_{12} \\ d_{12} \\ \vdots \end{bmatrix} = \frac{1}{\sqrt{2}} \begin{bmatrix} \cdots & & \cdots & & \cdots \\ & 1\ 1\ 0 & & 0\ 0\ 0 & \\ & 1-1\ 0 & & 0\ 0\ 0 & \\ & 0\ 0\ 1 & & 1\ 0\ 0 & \\ \vdots & & & & \vdots \\ & 0\ 0\ 1 & & -1\ 0\ 0 & \\ & 0\ 0\ 0 & & 0\ 1\ 1 & \\ & 0\ 0\ 0 & & 0\ 1-1 & \\ \cdots & & \cdots & & \cdots \end{bmatrix} \begin{bmatrix} \vdots \\ a_0 \\ a_1 \\ a_2 \\ a_3 \\ a_4 \\ a_5 \\ \vdots \end{bmatrix} \quad (1)$$

The same filtering operation is performed in the LL sub-band for the next level of the transform, whereas the other sub-bands (i.e., LH, HL and HH) can be stored, transmitted or discarded, being the transform coefficients related to higher-frequency components.

The third building block carries out the compression and extracts the desirable information from the 2D transform, e.g., LL component. The all-optical system ends with the encoding building block where the data stream is delivered through the optical channel [7].

The optical device chosen to implement the HT was a 3 dB asymmetric coupler, also known as a magic-T, depicted in Figure 4. The asymmetric coupler is characterized by having different waveguides widths, which can present a wide range of coupling ratios and low value of excess loss (0.7 dB),

including input and output single-mode fiber coupling losses [28].

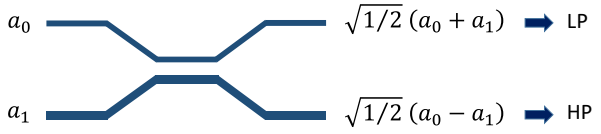

Figure 4. Scheme of a 3 dB asymmetric optical coupler.

To perform the HT operations the asymmetric coupler must be designed in order to perform a 50% coupling ratio.

B. PIC design for data compression

A data compression chip based on Haar wavelet transform was designed in accordance with the rules and using building blocks available from "Application Specific Photonic Integrated Circuit" (ASPIC) foundries [29], as well as proprietary building blocks created and simulated by the authors [4].

The chip was fabricated through a Multi-Project Wafer (MPW) offered by the consortium "Joint European Platform for Indium Phosphide based Photonic Integration of Components and Circuits" (JePPIX) [30].

This platform allows the development of low-cost ASPIC using generic foundry model and it supplies design kits for MPW. The fabrication process was achieved under the program "Photonic Advanced Research and Development for Integrated Generic Manufacturing" (PARADIGM) [31], developed to allow Universities to access to foundry processes. This program reduces the costs of the design, development and manufacture by establishing library-based design combined with technology process flows and design tools.

1) Asymmetric adiabatic coupler

An asymmetric adiabatic coupler in Indium Phosphide (InP) platform, based on adiabatic coupling arrangement was designed using the medium-index-contrast waveguide E600 structure, provided from Fraunhofer Gesellschaft Heinrich Hertz Institute (FhG-HHI) design manual structures [32].

Due to non-disclosure agreement (NDA) of Oclaro and HHI generic foundry processes, further details about the waveguide structure (e.g., structure dimensions and refractive indexes) cannot be provided. The wavelength supported by the developed structure is infrared C-band.

To achieve the phase and coupling ratios necessary for the asymmetric coupler requirements, extensive simulations and fine tuning of all design parameters were performed to attain the right profiles and outputs. Design and propagation analysis was conducted under the Beam Propagation Method (BPM) in OptoDesigner, a tool provided by Phoenix Software [33] [34]. The generic design of the developed InP asymmetric coupler is depicted in Figure 5.

A set of several sections of different sizes was applied in the waveguides design to guarantee the expected coupler behavior.

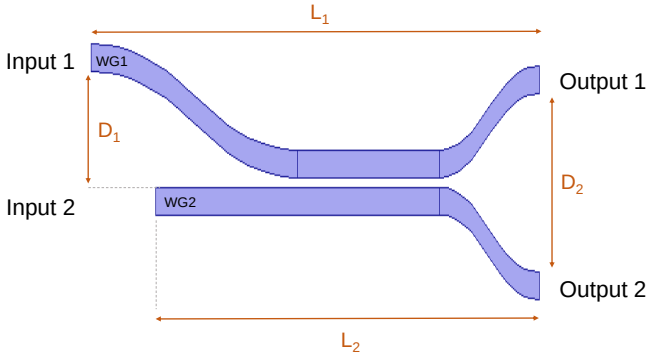

Figure 5. Diagram of the InP asymmetric adiabatic coupler composed by several sections of different sizes. The scheme diagram is not in scale.

A summary of the general dimensions of the coupler is presented in Table I.

TABLE I. GENERAL DIMENSION S OF THE ASYMMETRIC COUPLER

	Coupler dimensions	**(μm)**
D_1	Distance between input WG	40
D_2	Distance between output WG	70
L_1	Length of WG_1	2815
L_2	Length of WG_2	2264

WG: Waveguides. WG_1: Top waveguide from the coupler (waveguide 1). WG_2: Bottom waveguide from the coupler (waveguide 2).

The waveguides were composed by a set of different sections, such as straight, taper, and bend elements [35], as depicted in Figure 6.

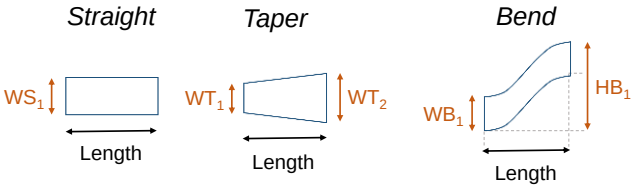

Figure 6. Diagram of three general elements that compose the different sections of the asymmetric coupler waveguide. The *taper* element is also applied in the mirror form, i.e., input as WT_2 and output as WT_1. The scheme diagram is not in scale.

The general dimensions of the elements provided in Figure 6 are presented in Table II.

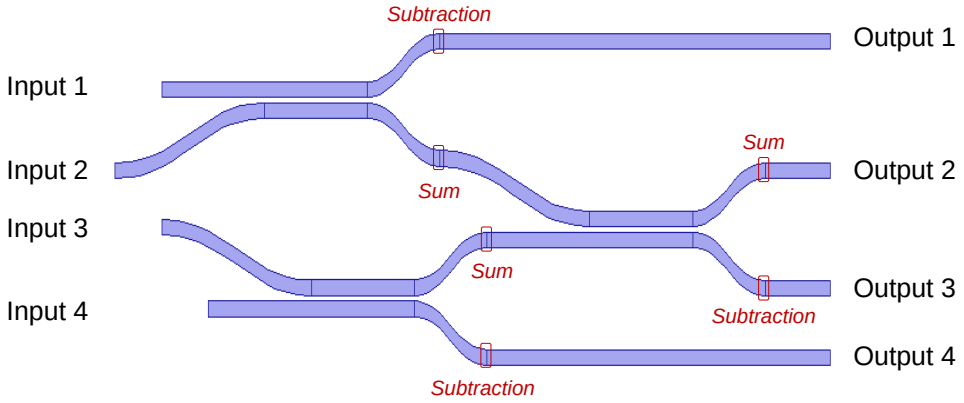

Figure 7. Diagram of the two level network composed by three InP asymmetric adiabatic couplers to perform the expect operations of the Haar wavelet transform.

TABLE II. GENERAL DIMENSIONS OF THE ELEMENTS THAT COMPOSE THE DIFFERENT SECTIONS OF THE ASYMMETRIC COUPLER

	Waveguide elements dimensions	**(μm)**
WS_1	Width of the *straight* element	1.15
WT_1	Input width of the *taper* element for WG_1	1.30
	Input width of the *taper* element for WG_2	1.00
WT_2	Output width of the *taper* element for WG_1 and WG_2	1.15
WB_1	Width of the *bend* element	1.15
HB_1	Height of the *bend* element for WG_1	5.00
	Height of the *bend* element for WG_2	3.60

WG: Waveguides. WG_1: Top waveguide from the coupler.
WG_2: Bottom waveguide from the coupler.

To perform the Haar wavelet transform a two levels network with three asymmetric couplers was designed, as depicted in Figure 7.

2) Chip design

An InP data compression chip to address the Haar wavelet transform was designed [4]. The optical chip is composed by four Distributed Feedback (DFB) lasers (L1-L4), three asymmetric couplers (C1-C3), six PIN photodiodes for network monitoring, two spot size converters, six multimode interferometers (MMI) 1×2 and one MMI 2×2. The e PIC includes one coupler network for compression and another one for decompression. The compression network is composed by the three asymmetric adiabatic couplers, arranged in a two level network, as depicted in Figure 7.

The inputs of the compression network are fed by four DFB lasers.

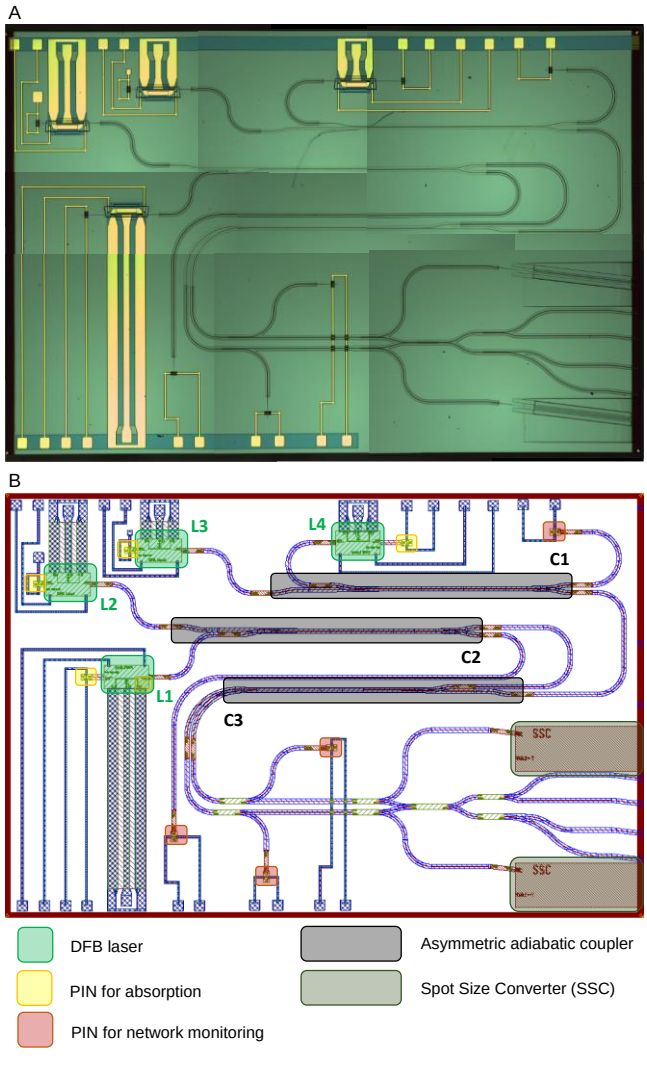

Figure 8. (A): Microscope image of the optical chip (with objective of 5×). (B): Design architecture of optical chip for data compression based on Haar wavelet transform.

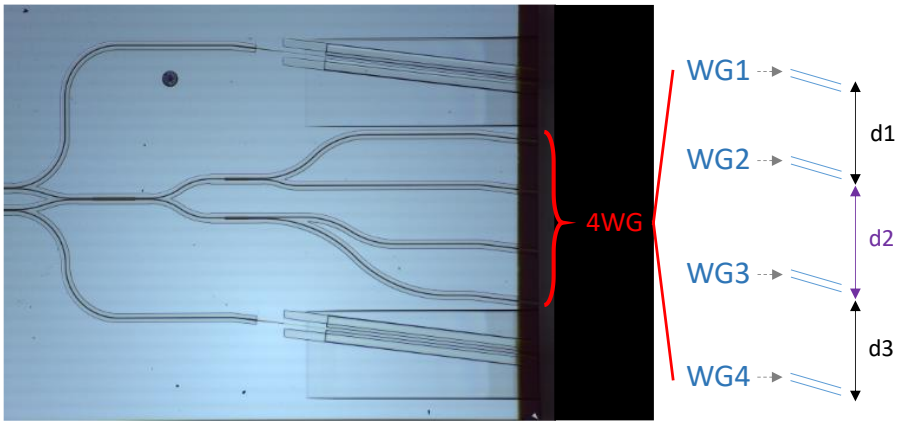

Figure 9. Measurements of the distance between the four waveguides (WG) at the end of the two level compression network.

The outputs are connected to two spot size converters (providing optical output signal) and PIN photodiodes (providing electrical output signal), see Figure 8.

The decompression network is composed by four MMI 1×2 and one MMI 1×1. Four optical outputs are provided, as depicted in the bottom right corner of Figure 8–B. The complete circuit architecture is presented in Figure 8.

The HT operations include Low-pass (L) and High-pass (H) filters applied over one dimension at a time. This filtering operation corresponds to the calculation of the average between two neighbors' pixels values (LP) or the difference between them (HP) [7]. The HT is implemented with a two level network composed by three asymmetric adiabatic couplers (2×2), reproducing the required operations, i.e., the average (sum) and the difference (subtraction) between the optical input pair [4].

The 2D HT can be decomposed in four sub-bands, LL, LH, HL and HH [7]. The LL gives the data compressed. In the chip these four sub-bands can be extrapolated from the four output waveguides (WG) at the end of the three asymmetric couplers network, as depicted in Figure 9.

The measurements of the distance between the four WG at the end of the three asymmetric coupler network are $d_1 = 241.3\ \mu m$, $d_2 = 278.6\ \mu m$, and $d_3 = 248.0\ \mu m$, see Figure 9. Measurements were performed with a Leica microscope (DM 750M; 1CC50 HD) and an objective of 20× (HI Plan EPI, 20×/0.40) [36].

BPM simulations from OptoDesigner of the asymmetric adiabatic coupler and the two level network are provided in *Results* subsection *A*.

C. Generation of the CGH

The CGH is a phase mask or diffractive optical element that can be displayed on an SLM [17].

The information to be transformed (in the Fourier domain) is introduced into the optical system by the SLM, with a phase mask that is appropriate to the input function of interest [37].

The following calculations applied for the generation of the CGH were based in the Fourier optical principles presented in [37].

The CGH was obtained with a linear phase mask calculated in the frequency domain (2), where c_x and c_y are the horizontal and vertical tilt parameters, respectively; and f_x and f_y are the components of the spatial frequency vector corresponding to the image to be generated in the X and Y axis, respectively.

$$M(f_x, f_y) = -2\pi(c_x f_x + c_y f_y) \quad (2)$$

The mask transfer function to be sent to the SLM, is given by $H_{mask} = M\left(f_x, f_y\right) mod 2\pi$, ensuring that the phase values are set in the range of $[-\pi, \pi]$.

A collimated Gaussian beam with transverse profile S_{in} is imaged onto the SLM via a lens. Using the Fraunhofer approximation this produces the Fourier transform at the SLM plane, $fft(S_{in})$. Next, this illumination profile is multiplied with the phase mask, $e^{iH_{mask}}$.

Finally, the result is Fourier transformed by a second lens through an inverse Fourier transform to give S_{out}, the field at the input plane of the PIC.

An estimation of the output signal is given by (3).

$$S_{out} = ifft(H(fft(S_{in})) \quad (3)$$

$$S_{in} = \exp\left(-\left(2\frac{x - x_0}{w_x\, log(\sqrt{2})}\right)^2 - \left(2\frac{y - y_0}{w_y\, log(\sqrt{2})}\right)^2\right) \quad (4)$$

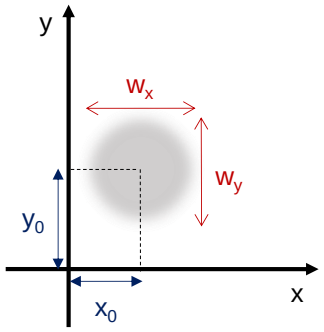

Figure 10. Diagram in Cartesian coordinate system describing the parameters (x_0, y_0) and (w_x, w_y) used for the estimation of the Input beam S_{in}.

S_{in} describes the signal of the input beam (4), where (x_0, y_0) provides the horizontal and vertical position and (w_x, w_y) the width and the height of the beam, respectively, as depicted in Figure 10.

1) *Optimization of the CGH*

To obtain a hologram that replicates the output of the four WG of the optical chip (see Figure 9) was computed a composite hologram of four beams by approximate phase-only superimposition of four independent holograms generated by (2). The correspondent linear transformations in the Fourier domain presented in (5), (6) were applied [1].

$$H = \angle(e^{iH_1} + e^{iH_2} + e^{iH_3} + e^{iH_4}) \quad (5)$$

$$H_1 = \exp\left(i2\pi\left(c_{x1}f_x + c_{y1}f_y\right)\right) \quad (6)$$

A phase-only SLM does not allow to simply address the inverse Fourier of the desired pattern into the far-field and replicate the resulting distribution of amplitude and phase directly on the SLM [13], thus it is challenging to spatially modulate the light with the expected resolution and accuracy.

To overcome this difficulty, an iterative algorithm to obtain the desired hologram with an error factor $\delta \leq 10\%$ was implemented. This threshold was set to avoid an infinite loop in the optimization algorithm, while ensuring an accuracy $\geq 90\%$ in the output result.

The main steps of the algorithm can be described as:

i) generate a 1st linear phase mask to produce the expected initial field based on (5);
ii) initially set the four values a_{1-4} to 1, from $H = \angle(a_1 e^{iH_1} + a_2 e^{iH_2} + a_3 e^{iH_3} + a_4 e^{iH_4})$;
iii) acquire the replay field form the hologram generated by SLM (I_{SLM}) with a camera and feed this data to the algorithm;
iv) calculate the difference between the hologram generated and the initial field expected, defined as error factor: $\delta = |I_{SLM} - I_1| \leq 0.1$;
v) if the condition $\delta \leq 0.1$ is not satisfied repeat steps (ii-iv) by iteratively adjusting the values of a_{1-4} to compensate the error factor.

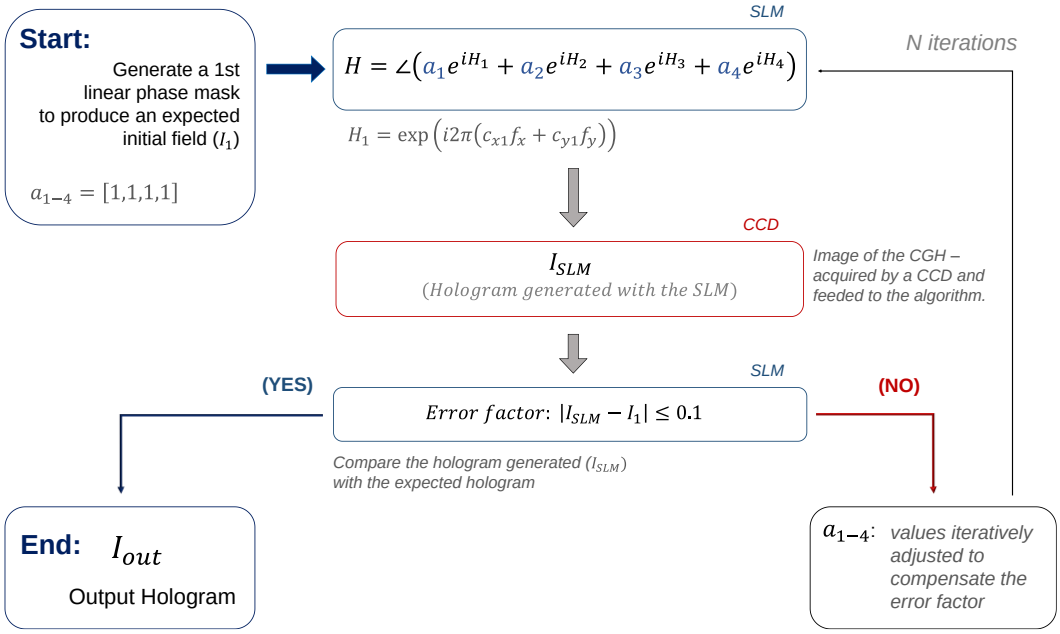

Figure 11. Block diagram of the algorithm applied for the optimization of the CGH.

The algorithm developed in Matlab® [38] was able to control both SLM and camera hardware. The block diagram of the algorithm is presented in Figure 11.

The error factor (δ) quantifies the deviation of the generated hologram when compared with the expected output of the optical chip, i.e., the dimensions of the four WG.

D. Setup to generate the CGH

A reflective LCoS phase only SLM, model PLUTO-TELCO-012, with a wavelength range of 1400-1700 nm, an active area of 15.36 mm × 8.64 mm, a pixel pitch of 8.0 µm, a fill factor of 92% and reflectivity of 80% [11] was used to display the hologram.

To remove the phase distortion and have the full Fourier transform scaled by the factor of the focal length (f) the optical system was design based in the $4f$ system configuration, i.e., four distances of length f separating the input plane from the output plane [37]. This forms the basis of a low distortion optical system.

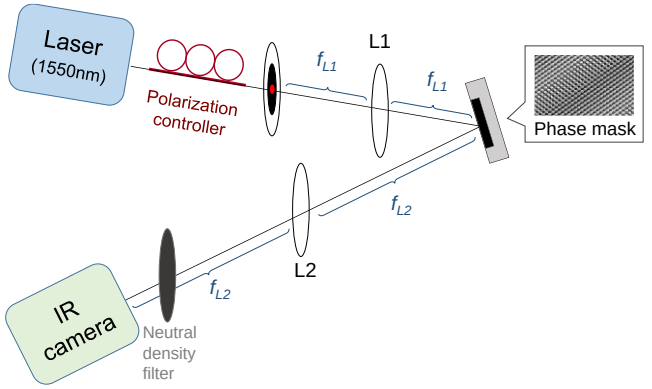

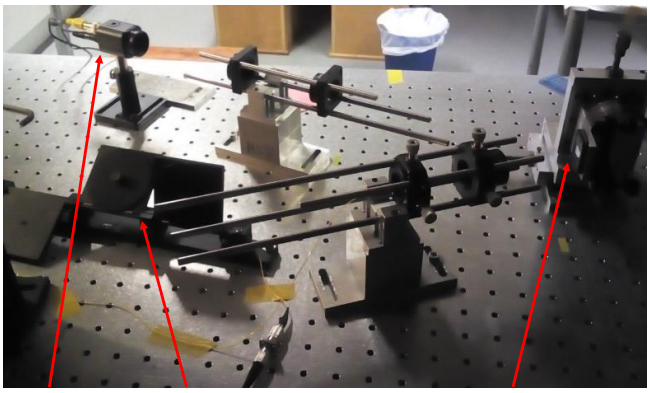

Figure 12. Top figure: Scheme of the hologram reconstruction system, using an infrared (IR) laser of 1550nm, a polarization controller, lens L1, a LCoS-SLM, lens L2 and a IR camera. Bottom figure: Photography of the setup presented.

The setup was composed of: a laser (1550 nm wavelength); a polarization controller; two lenses (AC254-050-C-ML, AR coating 1050-1620 nm) L1 and L2 with a focal length of 75 mm and 250 mm, respectively; a Near-Infrared (IR) (1460-1600 nm) camera (sensing area: 6.4×4.8 mm, resolution: 752×582, pixel size: 8.6×8.3 µm) to capture the hologram produced; and a neutral density filter to avoid saturation in the camera acquisition, see Figure 12.

III. RESULTS

The results section is divided in two subsections: (A) 2D BMP simulation results for the asymmetric adiabatic coupler; and (B) experimental CGH results.

A. BPM simulations

Light propagation simulations of the InP asymmetric adiabatic coupler with input signal in the: i) upper waveguide (WG_1); ii) lower waveguide (WG_2); and iii) same input signal in both WG_1 and WG_2; are presented in Figure 13 and Figure 14.

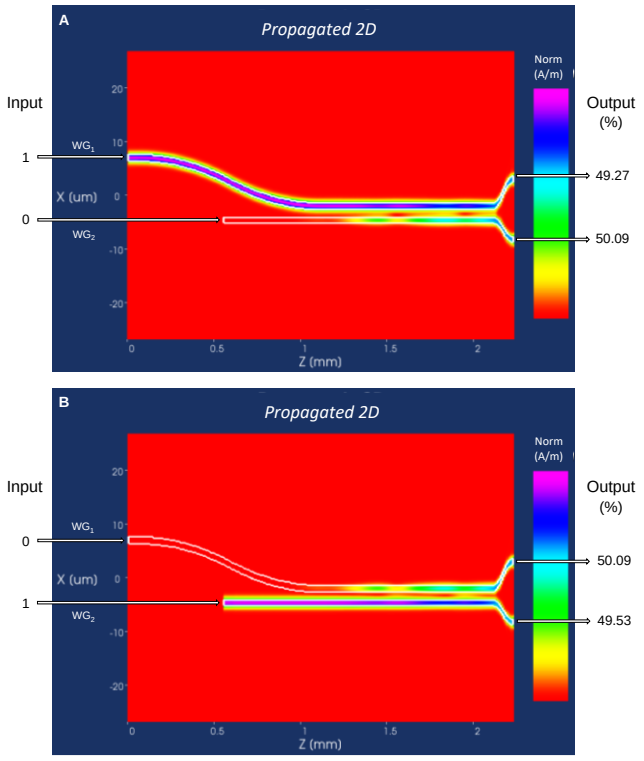

Figure 13. Power propagation in the asymmetric adiabatic coupler when fed with signal on: (A) upper waveguide (WG_1) and (B) lower waveguide (WG_2). Output power values are presented in percentage.

The simulation results demonstrate that the coupler is behaving as expected.

As depicted in Figure 13-A and Figure 13-B, the behavior as a 50% splitter is observed, when only one of the input waveguides carries an optical signal.

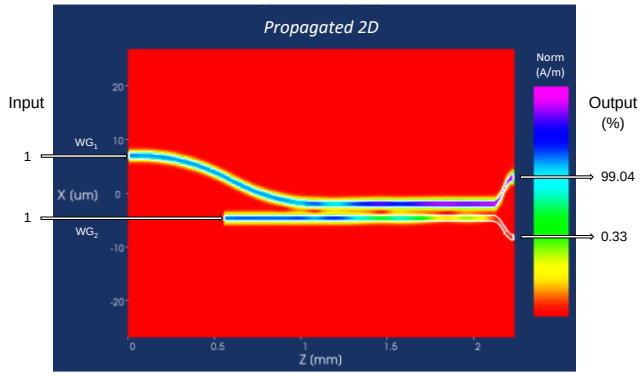

Figure 14. Power propagation in the asymmetric adiabatic coupler when the same input signal is provided on both WG_1 and WG_2. Output power values are presented in percentage.

When both of the input waveguides carry an optical signal, sum and subtraction are achieved at the output waveguides. As can be seen by the duplication of power in the WG_1 (99% of the output signal) and the absence of power in the WG_2 (0.3%), see Figure 14.

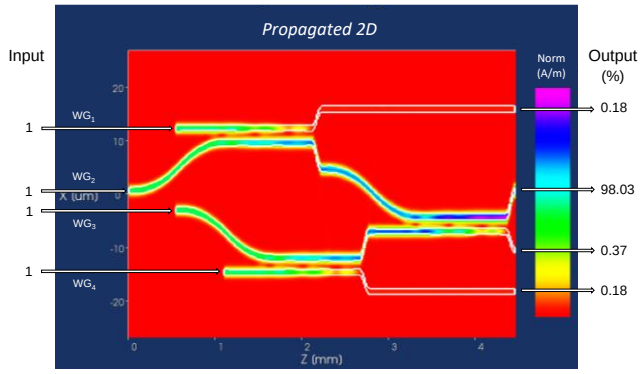

Figure 15. Power propagation for the two level network composed by three asymmetric adiabatic couplers. Output power values are presented in percentage.

The power propagation result for the two level network composed by three InP asymmetric adiabatic couplers is presented in Figure 15. As expected, the HT operations are carried out correctly, which can be confirmed by the power at the four output waveguide ports, i.e., sum at the output WG_2 (98% of the overlap output signal).

B. *Experimental CGH results*

A hologram was generated so as to produce four beam profiles in the first order of diffraction when displayed on the SLM.

Figure 16 presents the image acquired from the replay field of the hologram generated with the initial (I_1) and optimized (I_{out}) CGH.

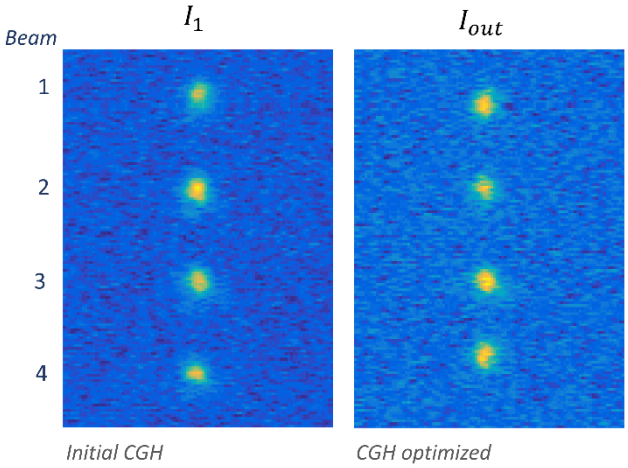

Figure 16. Replay field of the hologram acquired by the IR camera using an: i) initial hologram (left figure), and ii) optimized hologram (right figure).

The analysis of the obtained replay field images can be described by the following steps:

(1) calculate the intensity integration of the image matrix, i.e. sum of all elements along each line of the image matrix, depicted as S_{raw};
(2) application of the Savitzky-Golay (SG) filter to smooth the intensity integration signal obtained in step (1), depicted as S_{SG};
(3) implementation of a first order Gaussian fit curve to the filtered signal, depicted as *Gauss fit*;
(4) extraction of Gaussian parameters to calculate the distances between the four beams (obtained from the CGH) and compare with the expected results (d_1, d_2 and d_3 from the optical chip).

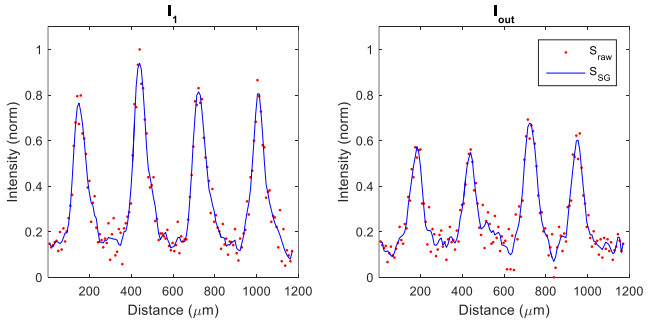

Figure 17. Integrated intensity from the replay field image S_{raw} (red dots), and correspondent smoothing with Savitzky-Golay (SG) filter S_{SG} (blue line). Left: Initial CGH; Right: Optimized CGH.

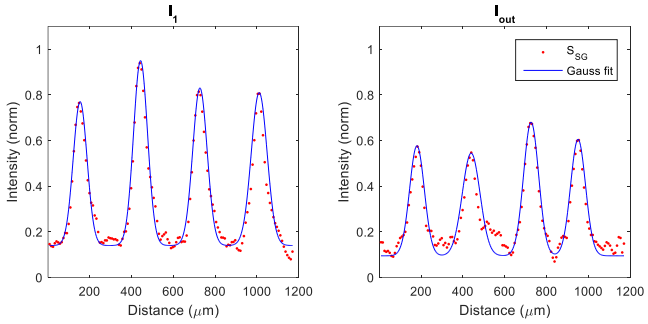

Figure 18. Gaussian fit (*Gauss fit* – blue line) of smoothed integrated intensity signal from the replay field image (S_{SG} – red dots). Left: Initial CGH; Right: Optimized CGH.

The signal smoothing of the intensity integration was obtained with the Savitzky-Golay filter, which can be characterized by a generalized moving average with filter coefficients determined by an unweighted linear least-squares regression and a polynomial model of specified degree [38]. The parameters applied in the filter were a polynomial order 9 and a window length 19.

Results after steps (1) and (2) are depicted in Figure 17, and Gaussian curve fitting application are presented in Figure 18.

The distance between the four beams was calculated from the center position of each beam profile, given by the Gaussian fit coefficient corresponding to the position of the center of the peak. The coefficients were obtained with 95% confidence bounds.

The deviation values (δ) of the generated hologram (i.e., initial I_1 and optimized I_{out} holograms) when compared with the expected output of the optical chip (i.e., d_1, d_2 and d_3 from Figure 9) are presented in Table III.

TABLE III. ERROR FACTOR (δ) VALUES FOR d_1, d_2, AND d_3

	Initial CGH (%)	**Optimized CGH** (%)
δ_{d1}	19.76	7.48
δ_{d2}	1.96	2.90
δ_{d3}	14.31	9.44

An error factor $\delta \leq 20\%$ was obtained for the initial CGH and $\delta \leq 9\%$ for the final optimized CGH.

Power measures of the beams were performed through the integration intensity profiles, i.e., the integral of the Gaussian fit. Table IV presents the integration of the intensity profiles for each beam when applying the initial an optimized CGH. Correspondent mean and standard deviation values of the beam profile for both cases are also provided.

TABLE IV. INTEGRATION OF THE INTENSITY PROFILES FOR THE FOUR BEAMS

Beam	**Initial CGH** (*u.a.*)	**Optimized CGH** (*u.a.*)
1	6.30	5.12
2	8.21	5.78
3	7.18	6.37
4	7.69	5.51
Mean	7.35 ± 0.81	5.69 ± 0.52
Std (%)	11.17	9.14

Integration of the normalized Gaussian fits presented in Figure 18. The four beams are numbered from 1 to 4 from top to down, as depicted in Figure 16. Std: Standard deviation.

A beam mean power loss of 1.1 dB between the initial and the optimized CGH was observed. Nonetheless, a better beam equalization was achieved in the optimized CGH with a standard deviation reduction of 2%.

IV. DISCUSSION

The design of the asymmetric adiabatic coupler and the all-optical network implemented to perform the Haar wavelet transform in InP were demonstrate to operate according to predictions as confirmed by the BPM simulations, supporting their feasibility for compression purposes.

An improvement in the generated hologram is achieved with CGH optimization, i.e., a major reduction of 11% (difference between initial and optimized) in the error factor (δ) was obtained. Nevertheless, the loss of 1.1 dB identified on the mean beam power for the optimized CGH an improved equalization between the beams was observed, with a 2% reduction in the standard deviation.

Algorithm improvements will be addressed to mitigate the power discrepancies between the four beams and optical artefacts associated with the diffraction of light not yet completely eliminated, which can cause a reduction of signal expected at the four output WG of the optical chip.

An alternative approach to correct some of this artefacts would be the implementation of the Gerchberg-Saxton [21] or simulated annealing [22] algorithms, nonetheless due to the power-loss (up to 9dB [13]) associated with these approaches they were not addressed in this study.

The phase mask that replicates the expected output of the optical chip can be used to multiplex/demultiplex the obtained result. Furthermore, a phase mask, which addresses the HT operations can also be applied to invert the compression induced by the HT (optically implemented in the chip with the three asymmetric couplers network).

The use of the SLM coupling platform will allow to provide a proof of concept of the PIC operation.

V. CONCLUSION

An extensive PIC characterization and testing is essential to provide an accurate prediction of its performance. In this study, we proposed a new concept to use the SLM as a flexible platform for feeding photonic integrated processors in order to complement the PIC characterization process. The capacity of the SLM to dynamically reconfigure light allows to feed and/or receive information to the PIC and can be used as a parallel implementation of the HT image compression algorithm. This data can be used to provide a proof of concept of the operation performed by the optical chip, e.g., 2D HT. The design of building blocks for the HT implementation as well as the all-optical network were proposed and simulated, demonstrating their viability for compression. A first result was obtained, i.e., a phase mask that can be used to receive the output of an optical chip for data compression based in the HT.

Further developments will be conducted to provide a more robust SLM based flexible coupling platform, e.g., by improving the optical system components and the implemented phase masks.

ACKNOWLEDGMENT

This work is funded by Fundação para a Ciência e a Tecnologia (FCT) under through national funds under the scholarships PD/BD/105858/2014 and SFRH/BPD/119188/2016; and the project COMPRESS - All-optical data compression – PTDC/EEI-TEL/7163/2014. Additional support was provided by the European Regional Development Fund (FEDER), through the Regional Operational Program of Centre (CENTRO 2020) of the Portugal 2020 framework [Project HeatIT with Nr. 017942 (CENTRO-01-0247-FEDER-017942)], and the COST action CA16220 European Network for High Performance Integrated Microwave Photonics (EUIMWP). The authors acknowledge PICadvanced and Patricia Lopes for their collaboration.

REFERENCES

[1] C. Pinho *et al.*, "Flexible Platform for Feeding Photonic Integrated Processors," in *The Thirteenth Advanced International Conference on Telecommunications (AICT 2017)*, 2017, pp. 1–4.

[2] Grand View Research, "Photonic Integrated Circuit (IC) Market Size Report," 2016.

[3] Credence Research, "Photonic Integrated Circuits Market," 2016.

[4] C. Pinho *et al.*, "Design and Characterization of an Optical Chip for Data Compression based on Haar Wavelet Transform," in *OFC 2017 - Optical Fiber Communication Conference*, 2017, vol. Part F40-O, p. Th2A.9.

[5] M. Smit *et al.*, "An introduction to InP-based generic integration technology," *Semicond. Sci. Technol.*, vol. 29, no. 8, p. 083001, 2014.

[6] V. Ashok, T. Balakumaran, C. Gowrishankar, I. L. A. Vennila, and A. N. Kumar, "The Fast Haar Wavelet Transform for Signal & Image Processing," *Int. J. Comput. Sci. Inf. Secur.*, vol. 7, no. 1, pp. 126–130, 2010.

[7] G. Parca, P. Teixeira, and A. Teixeira, "All-optical image processing and compression based on Haar wavelet transform," *Appl. Opt.*, vol. 52, no. 12, pp. 2932–2939, 2013.

[8] J. Carpenter, S. Leon-saval, B. J. Eggleton, and J. Schröder, "Spatial Light Modulators for Sub-Systems and Characterization in SDM," in *2014 OptoElectronics and Communication Conference and Australian Conference on Optical Fibre Technology*, 2014, pp. 23–24.

[9] H. J. Lee, H. S. Moon, S.-K. Choi, and H. S. Park, "Multi-core fiber interferometer using spatial light modulators for measurement of the inter-core group index differences," *Opt. Express*, vol. 23, no. 10, p. 12555, May 2015.

[10] Meadowlark Optics, "XY Spatial Light Modulator," 2015. [Online]. Available: https://www.meadowlark.com/xy-spatial-light-modulator-p-119. [Accessed: 22-Nov-2017].

[11] Holoeye, "Spatial Light Modulators," *Holoeye Photonics AG*, 2013. [Online]. Available: http://holoeye.com/spatial-light-modulators/. [Accessed: 22-Nov-2017].

[12] Department of Physics, "An Introduction to Spatial Light Modulators," *Stony Brook University*, 2013. [Online]. Available: http://laser.physics.sunysb.edu/~melia/SLM_intro.html. [Accessed: 22-Nov-2017].

[13] J. Carpenter, "Holographic Mode Division Multiplexing in Optical Fibres," University of Cambridge, 2012.

[14] G. Lazarev, A. Hermerschmidt, and S. Kr, "LCOS Spatial Light Modulators : Trends and Applications," *Opt. Imaging Metrol. Adv. Technol.*, pp. 1–29, 2012.

[15] Hamamatsu, "Phase spatial light modulator LCOS-SLM," in *Handbook LCOS-SLM*, 2012, pp. 1–14.

[16] M. Kovachev *et al.*, "Reconstruction of Computer Generated Holograms by Spatial Light Modulators," *Multimedia Content Representation, Classification and Security*, vol. 4105. Springer Berlin Heidelberg, pp. 706–713, 2006.

[17] C. Pinho, A. Shahpari, I. Alimi, M. Lima, and A. Teixeira, "Optical transforms and CGH for SDM systems," in *18th International Conference on Transparent Optical Networks (ICTON 2016)*, 2016, pp. 1–4.

[18] L. B. Lesem, P. M. Hirsch, and J. A. Jordan, "The Kinoform: A New Wavefront Reconstruction Device," *IBM J. Res. Dev.*, vol. 13, no. 2, pp. 150–155, Mar. 1969.

[19] Y. Torii, L. Balladares-Ocana, and J. Martinez-Castro, "An Iterative Fourier Transform Algorithm for digital hologram generation using phase-only information and its implementation in a fixed-point digital signal processor," *Optik (Stuttg).*, vol. 124, no. 22, pp. 5416–5421, 2013.

[20] O. Ripoll, V. Kettunen, and H. P. Herzig, "Review of iterative Fourier-transform algorithms for beam shaping applications," *Opt. Eng.*, vol. 43, no. 11, pp. 2549–2556, 2004.

[21] R. Gerchberg, W. O. Saxton, B. R. W. Gerchberg, and W. O. Saxton, "A Practical Algorithm for the Determination of Phase from Image and Diffraction Plane Pictures," *Optik (Stuttg).*, vol. 35, no. 2, pp. 237–246, 1972.

[22] J. Carpenter and T. D. Wilkinson, "Graphics processing unit–accelerated holography by simulated annealing," *Opt. Eng.*, vol. 49, no. 9, pp. 095801-7, 2010.

[23] K. Deb, M. S. Al-Seraj, M. M. Hoque, and M. I. H. Sarkar, "Combined DWT-DCT based digital image watermarking technique for copyright protection," in *7th International Conference on Electrical and Computer Engineering*, 2012, pp. 458–461.

[24] C. Christopoulos, A. Skodras, and T. Ebrahimi, "The JPEG2000 still image coding system: an overview," *IEEE Trans. Consum. Electron.*, vol. 46, no. 4, pp. 1103–1127, 2000.

[25] K. S. Thyagarajan, *Still Image and Video Compression with MATLAB*. Hoboken, NJ, USA, NJ, USA: John Wiley & Sons, Inc., 2011.

[26] M. Vetterli, J. Kovačević, and V. K. Goyal, *Foundations of signal processing*. 2014.

[27] J. Kovacevic, V. K. Goyal, and M. Vetterli, *Fourier and Wavelet Signal Processing*, no. October. 2013.

[28] A. Takagi, K. Jinguji, and M. Kawachi, "Design and fabrication of broad-band silica-based optical waveguide couplers with asymmetric structure," *IEEE J. Quantum Electron.*, vol. 28, no. 4, pp. 848–855, Apr. 1992.

[29] G. Gilardi and M. K. Smit, "Generic InP-Based Integration Technology : Present and Prospects," *Progress In Electromagnetics Research*. 2014.

[30] JePPIX, "Joint European Platform for InP-based Photonic Integrated Components and Circuits." [Online]. Available: http://www.jeppix.eu.

[31] PARADIGM, "Photonic Advanced Research and Development for Integrated Generic Manufacturing," *May 29, 2014, PARADIGM and EuroPIC consortia*. [Online]. Available: http://www.paradigm.jeppix.eu/.

[32] JePPIX, "PARADIGM/EuroPIC Design Manual." PARADIGM and EuroPIC consortia, p. 232, 2014.

[33] Phoenix Software, "OptoDesigner 5 - The ultimate Photonic Chip Design environment," 2016. [Online]. Available: http://www.phoenixbv.com/index.php. [Accessed: 07-Feb-2018].

[34] PhoeniX Software, "User Manual OptoDesigner - version 5.0.7." p. 1825, 2015.

[35] PhoeniX BV, "User Manual OptoDesigner PhoeniX Software, version 5.1.4." p. 2913, 2017.

[36] Leica Microsystems, "Leica Application Suite," *Http://Www.Leica-Microsystems.Com/*, 2015. [Online]. Available: http://www.leica-microsystems.com/products/microscope-software/life-sciences/las-easy-and-efficient/. [Accessed: 04-Sep-2016].

[37] J. W. Goodman, *Introduction to Fourier Optics*, 2nd ed. Stanford: McGraw-Hill Companies, 1996.

[38] The MathWorks, "MATLAB - The language of technical computing." 2015.